Overstrain in flush optimal-chamfered cross-bored cylinders

J M Kihiu, G O Rading and S M Mutuli

Proceedings of the Institution of Mechanical Engineers, Part C: Journal of Mechanical Engineering Science 2006 220: 15
DOI: 10.1243/095440605X69903

Overstrain in flush optimal-chamfered cross-bored cylinders

J M Kihiu*, **G O Rading,** and **S M Mutuli**
Department of Mechanical Engineering, Jomo Kenyatta University of Agriculture and Technology, Nairobi, Kenya

The manuscript was received on 11 May 2005 and was accepted after revision for publication on 26 August 2005.

DOI: 10.1243/095440605X69903

Abstract: A three-dimensional finite-element method computer program was developed to establish the elastic–plastic, residual, and service stress distributions in cylinders with flush and non-protruding optimal-chamfered cross-bores under internal pressure. Eight-noded brick and four-noded tetrahedral isoparametric elements and the displacement formulation were used. The incremental theory of plasticity with a 5 per cent yield condition and von Mises yield criterion were assumed. The incipient and 5 per cent overstrain (ov) pressures were established for various thickness ratios and cross-bore to main bore radius ratios. For the optimum chamfer angle geometrical configuration, the stresses were determined for varying ov. The maximum and minimum effective stresses were located 7.5° from the meridional and transverse planes, respectively. Meridional plane through thickness yielding occurred at an ov of 41 per cent. The service stress gradients at the cross-bore chamfer end increased with ov for ovs >30 per cent. Stress reversals were eliminated for overstrain >27 per cent. Alternative autofrettage and yield condition procedures were proposed.

Keywords: elastic–plastic, residual stress, service stress, overstrain, autofrettage

1 INTRODUCTION

The earliest use of pressure vessels for steam generation was in 1698 [**1**], with an operating pressure of ~7 lbf/in^2. Higher pressures were used later, after the improvement of materials. Lack of simultaneous redesign of pressure vessels resulted in several catastrophic failures [**2**]. Some uses of pressure vessels, such as in isostatic compaction of metallic and ceramic powders, involves pressure as high as 300 MPa [**3**]. With pressure vessels holding high potential energy, minimizing accidental losses due to poor designs that may result from inadequate understanding of stresses is important. Pressure vessels usually have side openings for relief, safety valves, etc. [**4**], which introduce geometric discontinuities on its body. The intersection of the cross-bore and the cylinder bore forms a stress singularity curve having high relative stresses and sharp stress gradients [**5**]. The pressure-carrying capacity of such vessels, therefore, falls below that of a plain cylinder. For lower stresses, it has been a practice to introduce a radius at the cross-bore entry [**6**]. Chamfering has also been suggested, although little has been done to provide the optimal chamfer geometry. Understanding stress distributions in the regions of high stress would lead to the use of low safety factors, economy of materials, enhanced operating life, operational efficiency, improved failure diagnosis, and a reduction of losses due to failures.

Limitations of strength and ductility prevent use of high factors of safety [**7**], and therefore, a true representation of the state of stress in the presence of cross-bores is needed. The ASME Boiler and Pressure Vessel Code does not enforce a detailed stress analysis but only sets the wall thickness necessary to keep the basic hoop stress below an allowable stress. The higher localized stresses are implicit in the safety factor and design rules [**8**], assuming that any localized yielding in ductile materials results in stress redistribution. This code provides a quick design procedure, but is inadequate for cylinders with cross-bores having complex entry geometry and

**Corresponding author: Department of Mechanical Engineering, Jomo Kenyatta University of Agriculture and Technology, PO Box 62000, Nairobi 00200, Kenya.*

more so when autofrettaged. Pressure vessels are normally subjected to leak test pressures of 1.25–1.5 times the design pressure during commissioning [**9**]. This overstrain (ov) pressure causes yielding of the most highly stressed parts of the structure. In this work, ov is defined as the ratio of the distance between the yield radius and the main bore to the cylinder thickness. Overstrain pressure is the pressure that causes this level of ov. After the release of the pressure, residual stresses are left in the structure. For cylinders with chamfered cross-bores, it is important to establish the exact relationship between the ov pressure and the residual and service stresses. The nature of the resultant stress distributions is also important. The economic use of cylinders depends on the small controlled permanent deformations that occur [**6**]. Autofrettage is often done during manufacture when pressure greater than the leak test pressure is applied. This process results in higher residual stresses and a stronger cylinder, with service stresses being more uniformly distributed [**10**]. In the presence of cross-bores with complex entry geometry, this distribution is not obvious and a detailed analysis is necessary.

2 LITERATURE

Bursting pressure and ov studies to determine the pressure-carrying capacity of plain cylinders [**11**] have led to models for computing expansion and bursting strengths, based on tension and torsion data. For various steels, it has been shown that heat treatment has no effect on ov or bursting pressure [**12**]. Pressure combined with thermal treatment can produce a compressive residual stress in the inner and outer parts of tubes, applicable in the bend regions where stress-corrosion cracking is a problem [**13**]. The most comprehensive theoretical study involved a stiffness method for the solution of elastic–plastic problems [**14**]. This concept enabled the equilibrium equations to be expressed in terms of displacements and removed the need to trace the expansion of the elastic–plastic boundary during the actual solution of the differential equations. The method was not suitable for perfectly plastic or very small degree of hardening materials. The plastic stress–strain matrix, derivable by inverting the Prandtl–Reuss equations, is used for the solution of continuum elastic–plastic problems using the finite-element method (FEM) [**15**]. The method uses small and varying increments of load, just sufficient to cause a yield in successive elements, and has greatly reduced the programming effort in the incremental theory of plasticity. Other FEM solutions to three-dimensional elastic–plastic problems illustrating the applicability of the isoparametric elements and the order of computation times involved have been presented [**16**].

The effect of yield stress and strain hardening exponent of the material on the stress and strain levels has been studied in pipe bore expansions using the FEM [**17**]. By considering that the effective stress and its approximation are given by

$$\overline{\sigma} = Y_s + C\overline{\varepsilon^n} \tag{1}$$

$$\overline{\sigma} \approx C\overline{\varepsilon^n} \tag{2}$$

where $\overline{\sigma}$ and $\overline{\varepsilon^n}$ are the uniaxial test effective stress and strain, respectively, C the material constant, n the strain hardening exponent, and Y_s the yield stress of the material. The indeterminacy of the initial condition is, therefore, eliminated. The FEM has also been used in metal forming problems where finite size deformations introducing instability have been taken care of by modifying the stiffness formulation by means of the mean normal technique [**18**]. The yield theories of von Mises and Tresca have been compared in conditions of compressibility and incompressibility for elastic–plastic analysis of cylinders [**19**]. Large differences in stress were observed from these two criteria. A closed-form theory to include the Hencky stress–strain relations, incompressibility, and Ludwik strain hardening function was proposed. However, the work does not discuss which of the two criteria is more accurate.

Three-dimensional FEM analysis for chamfered cross-bored cylinders with $k = 1.4$ and 2, ca $= 45^\circ$, clr $= 0.25$, and $d = 0.12$ have been conducted [**20**], with few elements in the vicinity of the points of peak stresses and adjacent to the boundary being allowed to yield. Plastic strain components in the critical region of the cross-bore were determined. The author was mainly interested in fatigue life and no detailed data were provided. Three-dimensional analysis of plain cross-bored cylinders in partial autofrettage was carried out using the boundary element (integral) method [**21**] for $k = 2$ and 2.25 and $d = 0.25$. Autofrettage was performed after the introduction of the cross-bore. The maximum ov possible was found to be 35 and 27.5 per cent for $k =$ 2 and 2.25, respectively. The work did not cover enough cylinder–cross bore configurations. An optimum ov radius has been proposed [**22**] as being equal to $(R_i R_0)^{1/2}$ for medium-strength steels and slightly less for high-strength steels.

Aproximate equations suitable for a numerical solution of an axisymmetric shell under axisymmetric loadings have been developed [**23**]. An incremental approach under the consideration of the first-order approximation in determining the tangent stiffness characteristics of the finite element was used. The effects of isotropic and kinematic strain hardening

were included. Initial stresses were included to account for instability and large accumulated deformations during the loading of the structure.

Autofrettage has been found useful in increasing the fatigue life of high-pressure piping, compressor chambers, and similar components [**24**]. Determination of residual stresses arising from forming, cold working, or ov procedures is important, particularly where cross-bores may exist. For monoblock plain cylinders under partial autofrettage, the analytical residual stresses may be obtained directly by applying an equivalent thermal load [**25**]. Simple destructive methods based on fracture mechanics have been developed for measuring residual stresses [**26**], though they are not satisfactory for measuring the residual stress distributions where stress gradients are high. Sequential and selective destructive procedures employing incremental strain gauge data in FEM algorithms to construct the initial residual stress distribution are currently in use [**27**]. Tensile residual hoop stresses are introduced in seamless gas cylinder necks at the bore during the heat treatment stage. At the neck, the outer surface experiences compressive hoop stresses and the bore experiences tensile hoop stresses. Material removal corrective procedures to remove the bore residual stresses have been established [**28**]. As a means of measuring autofrettage in thick-walled cylinders, an experimental method based on measuring the hoop strain while axisymmetrically releasing the residual stress field by introduction of radial cuts in the cylinder has also been proposed [**29**]. This is due to the fact that access to the cylinder inside surface for purposes of placing strain gauges is usually denied.

Closed-form solutions of residual stresses in autofrettaged steel tubes are available [**30**]. Models neglecting both strain hardening and Bauschinger effects overestimate the bore residual hoop stress by 46 per cent whereas models including the Bauschinger effect only underestimate this value by 25 per cent . Analytical residual stresses for hardening and non-hardening materials considering the yield criteria of Tresca and von Mises have been obtained [**31**] by using closed and open-ended cylinders. The optimum ov to prevent reverse yielding has been proposed, and the ov found to prevent a reduction in fatigue life for cylinders with $k > 2.96$. The Tresca's yield criterion results were admissible for $k < 2$, but the von Mises citerion was found more practical for $k > 2$. The influence of strain hardening on open cylinders is important when $k \geqslant 3$. Linear elastic solutions can be used as a basis to generate an inelastic solution, which may then be used to predict the residual stress fields [**32**]. The dependency of the Bauschinger effect on plastic strains makes significant changes to residual hoop stress near the bore for low-level autofrettage, but this dependency is found to be insignificant for high-level autofrettage.

The evaluation of residual stresses inside the material or in very small cross-bores is difficult without a destructive procedure. Though a lot of work has been dedicated to the evaluation of residual stresses in cylinders, very little design or operational data are available in the research literature for the case of chamfered cross-bores. The FEM is a suitable tool because no destructive procedures are involved and the state of residual stress at any location can be determined. A knowledge of the stress levels and distributions is important. The aim of this work is to investigate the ov stress levels and the residual and service stresses for varying ov in chamfered cross-bored cylinders with an optimum chamfer angle (ca).

3 PROCEDURE

A three-dimensional FEM computer program in FORTRAN code was developed to carry out the elastic–plastic analysis [**5**] of optimal-chamfered cross-bored cylinders. The program was successfully used and yielded accurate results [**10**, **33**–**38**]. The quarter cylinder geometry for the structure is shown in Fig. 1. The displacement formulation was adopted and eight-noded brick and four-noded tetrahedral isoparametric elements were used. The tetrahedral elements were used only on the chamfer surface.

The pressure loads for various ov are shown and discussed elsewhere in section 4. Pressure is assumed to act normally on the cross-bore, chamfer, and cylinder main bore surfaces. A uniform stress given by [**5**]

$$\text{Stress} = \frac{\text{internal pressure}}{k^2 - 1} \tag{3}$$

which is applicable for closed-end cylinders, is assumed to act across the cylinder section in the far field. The displacement boundary conditions are

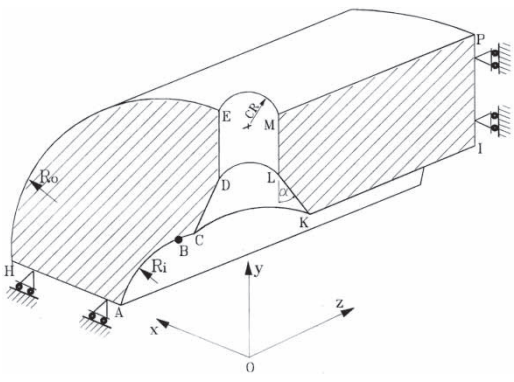

Fig. 1 Main dimensions of chamfered cross-bored cylinder

such that: $u_x = 0$ at $x = 0$; $u_y = 0$ at $y = 0$; $u_z = 0$ at $z = 0$.

The configuration was subdivided into five parts A1, A2, A3, A4, and A5 as shown in Fig. 2. The inputs were inner radius (75 mm), outer radius, length of line JI (nine times the cylinder length), radius of cross-bore, ca, and chamfer length. In part A1, the number of elements was input for lines DE (8), EF (6), and arc EM (12). For line DE, this was the minimum for the smallest k cylinder. The geometric ratios for lines DE (1.5) and EF (2.5) were also input. In part A2, the number of elements along chamfer line CD (6) was input. This was the minimum for the shortest clr. In part A3, the number of elements along line KJ (4) was input as well as the angle BO′C (10 per cent of the angle AO′C). In part A4, the number of elements along line JI (3) was input together with the geometric ratio (4). In part A5, the number of elements (6) and geometric ratio (0.8) along arc AB were also input. This resulted in a structure with 3087 nodes, 2652 elements, 9261 degrees of freedom, and a frontal width of 771. The global stiffness matrix coefficients computer memory requirement was reduced by 99.3 per cent . The aforementioned data completely defined the geometry. Geometric ratios were used in controlling the element aspect and volume ratios and were also employed where high stress gradients were anticipated. The choice of the number of elements and geometric ratios in each division was based on: for parts away from the cross-bore, to ensure that the far field stresses were close to the exact solution of a plain cylinder and in the cross-bore areas, to ensure that the elastic stress concentration factor reasonably converged while minimizing the frontal width and processing time [**5**]. The pressure vessel material was a high-strength SA-372 steel having a yield stress of 450 N/mm^2, a Poisson's ratio of 0.29, and a Young's modulus of 209×10^3 N/mm^2 [**39**]. To obtain the displacements, and Gauss point strains and stresses, the frontal solution technique [**40**] was employed.

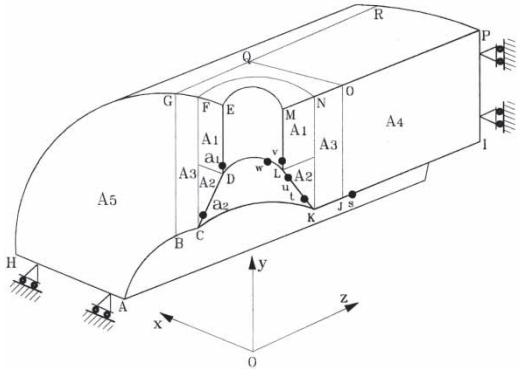

Fig. 2 Main discretization scheme

In the elastic–plastic range, the incremental theory of plasticity and the plastic stress–strain constitutive matrix were used [**15**]. Stress projection and nodal averaging followed by tensor transformation techniques [**41**] were employed to obtain cylindrical coordinate stresses for the nodal arrays.

An elastic perfectly plastic material obeying von Mises yield criterion was assumed. The Bauschinger effect was not included because reverse yielding was not allowed. During ov, any element that attained an effective stress within 5 per cent of the material yield stress was considered to have yielded [**15**]. This procedure had the effect of introducing some insignificant errors, but it reduced the number of loading cycles necessary before a given ov was achieved. A more stringent yield condition of 0.5 per cent had been demonstrated previously to assess the associated ov processing time factors [**37**]. Various ov levels were considered. For stress evaluation, $k = 3$, $d = 0.05$, clr $= 0.25$, and ca $= 11.5^\circ$ were used. For other k and d at clr $= 0.25$, the corresponding optimal ca [**5**] was used. The clr of 0.25 resulted in reasonable stress influences while avoiding undue weakening of the structure.

4 RESULTS AND DISCUSSION

4.1 Overstrain stresses

Figure 3 shows the transverse plane ov stresses at ov $= 5$ per cent and for an internal pressure of 117 N/mm^2. The radial stress starts at point B, having a value of about -112 N/mm^2, with the curve tending to 0 at point E, although at this point

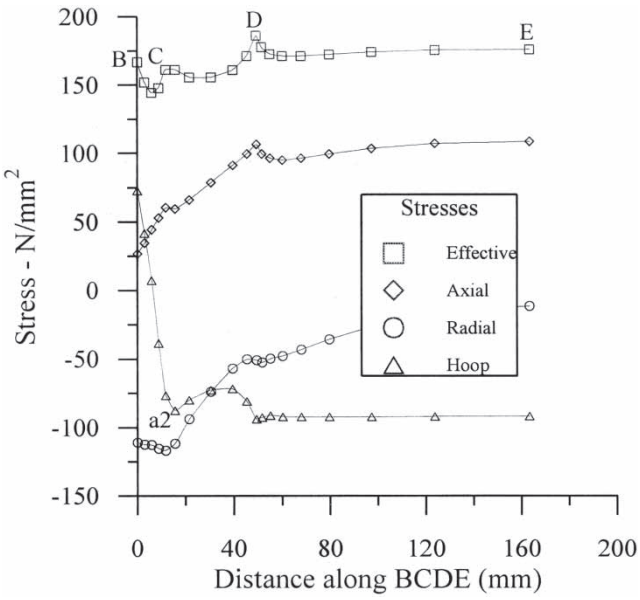

Fig. 3 Transverse stresses at ov $= 5$ per cent

the value is about $-12\ \mathrm{N/mm^2}$. It might be expected that this stress should have a value of 0 at point E, but it is important to realize that around the cross-bore, the radial, hoop, and axial stresses do not correspond to the principal stresses because the state of stress is very complex. There also exist shear stresses in this area which are absent in the far field. Around the chamfered area and the cross-bore, the axial stress is the most significant positive stress. This stress starts at point B having a value of $25\ \mathrm{N/mm^2}$ and rises to a maximum value of $108\ \mathrm{N/mm^2}$ at point D. Points D and E have the same value of axial stress. The hoop stress starts at point B having a value of $25\ \mathrm{N/mm^2}$ and drops sharply to a value of $-84\ \mathrm{N/mm^2}$ at point a2. This value remains constant between points D and E. The hoop stress has equal values at points a2, D, and E. From the effective stress curve, point D, is the most critical, with a maximum stress of $182\ \mathrm{N/mm^2}$. However, between points a1 and E, the effective stress is $175\ \mathrm{N/mm^2}$ and, therefore, points D and E are equally critical for this value of ov.

Figure 4 shows the meridional plane ov stresses at ov = 5 per cent. The radial stress has a zero value between points L and M and has a minimum value of $-112\ \mathrm{N/mm^2}$ at point J. The axial stress has a minimum value of $-82\ \mathrm{N/mm^2}$ at point K and this value prevails between points L and M. The hoop stress has a maximum value of $345\ \mathrm{N/mm^2}$ at point t and a local maximum at point L. Because the distance between the points of maximum hoop stress has decreased (from the elastic analysis [**5**]), it might be expected that as ov increases, this distance decreases, with the point of maximum hoop stress

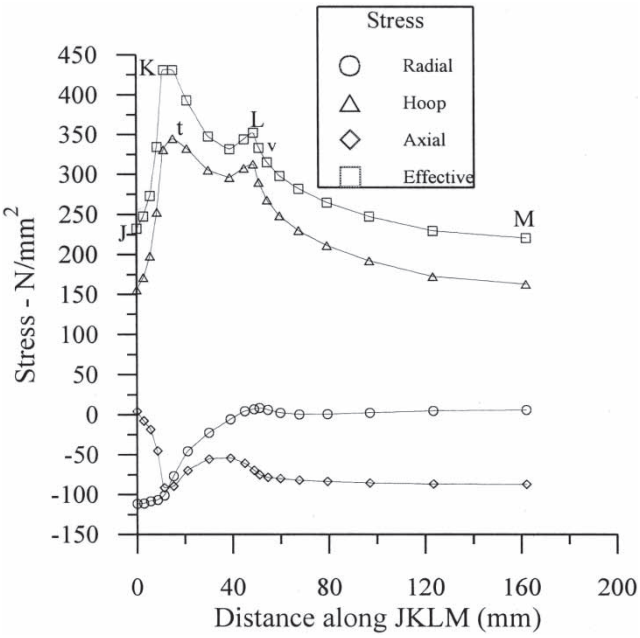

Fig. 4 Meridional stresses at ov = 5 per cent

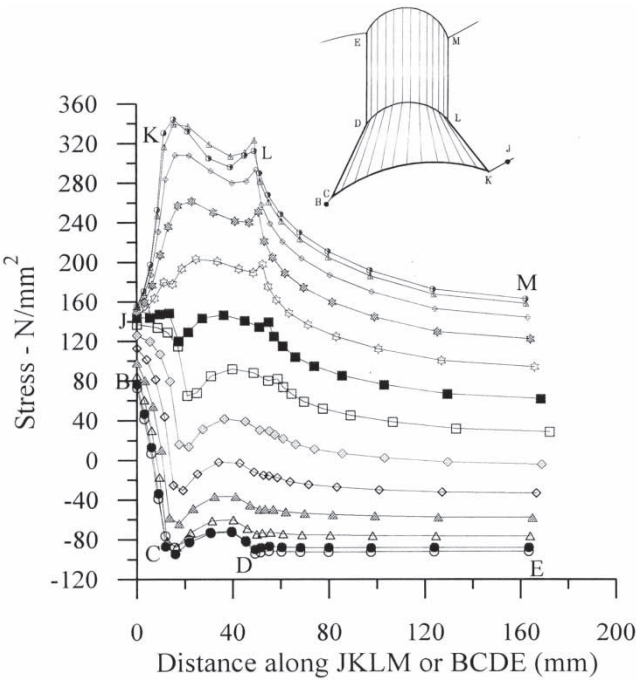

Fig. 5 Cross bore surface hoop stresses at ov = 5 per cent

around point K approaching point L until all the nodes have yielded. Contrary to observations from the elastic analysis [**5**], where points K and v have equal hoop stresses, the stresses now have different values, with the values at point K having risen more rapidly. Point K, which is in an element that has yielded, has a maximum effective stress of $430\ \mathrm{N/mm^2}$, lower than the material yield stress. This is due to structural discretization, where

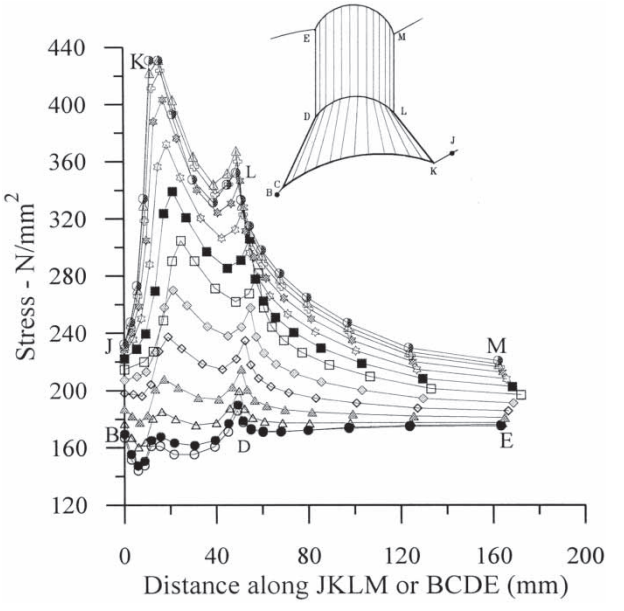

Fig. 6 Cross bore surface effective stresses at ov = 5 per cent

different element types sharing the same node as point K have not yielded. Stress projection and averaging techniques as employed in this work thereby result in an effective nodal stress lower than the material yield stress. It is expected that using the brick elements alone would result in effective stresses equal to the yield stress because tetrahedral elements are less accurate. Point v has a lower effective stress than point L.

The cross-bore surface ov hoop stresses are shown in Fig. 5. The stress patterns are similar to the elastic hoop stress patterns, particularly for planes around the transverse plane [**5**]. The stress levels are higher in both the positive and negative sense. Figure 6 shows the cross-bore surface effective stresses. The profiles are similar to those of elastic analysis of the same configuration, with the range of effective stress along curve EM being much lower than that along curve KC. Between points t and w, the set of nodes lying within 7.5° from the meridional plane have higher hoop stresses than those along the meridional plane. This was also noted in the case of elastic analysis. It is then possible to construct an ellipsoidal envelope enclosing points vLwtK, which prescribes the highest hoop stress points. Similar stress behaviour is observed in the transverse plane between points Ca2Da1. Between points C and D, the minimum hoop stress occurs in the nodes at 7.5° from the transverse plane. The reason behind this phenomenon is not well understood. Further analysis to better understand this observation was carried out and the results are shown in Figs 7 to 10. This involved observing the effective stresses of nodes lying within 22.5° from the meridional plane as ov was increased. Between points L and K, the

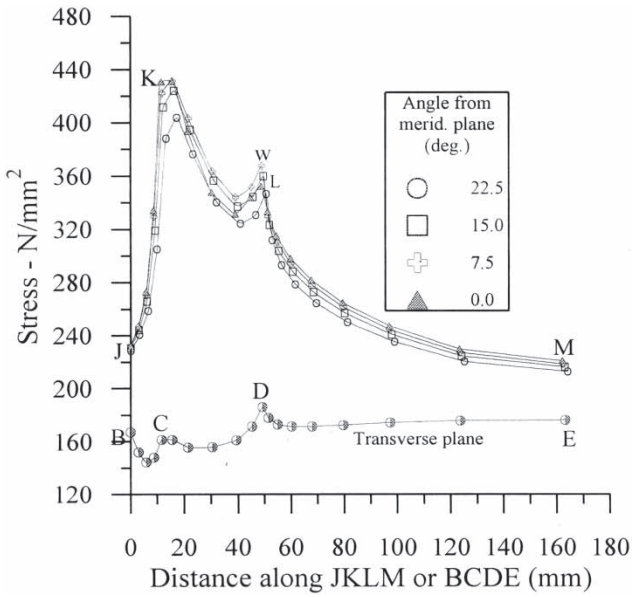

Fig. 7 Meridional effective stresses at ov = 5 per cent

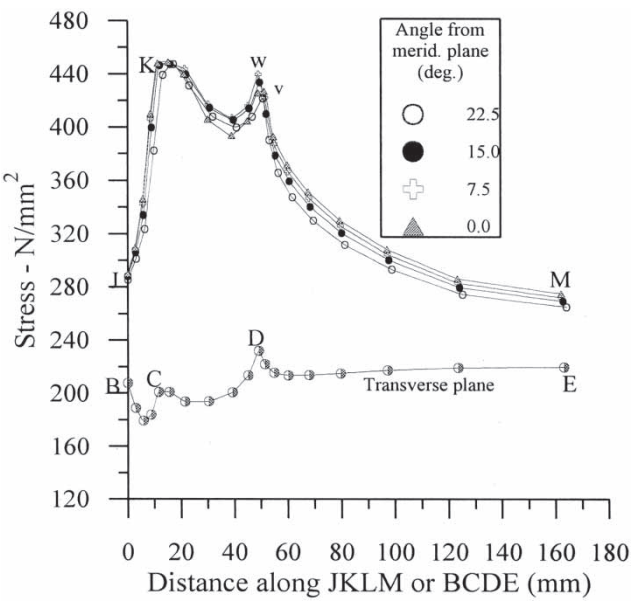

Fig. 8 Meridional effective stresses at ov = 25 per cent

nodes with angles within 15° of the meridional plane have higher effective stresses, although the maximum effective stress remains at point K. The point w, which is within 7.5°, remains a point of local maximum effective stress up to ov = 25 per cent and as the angle increases to 22.5°. The effective stress for nodes between points K and L relatively decreases as ov increases. The transverse plane effective stress remains relatively low with point D always having the highest effective stress. This shows that geometrical singular point edge effects

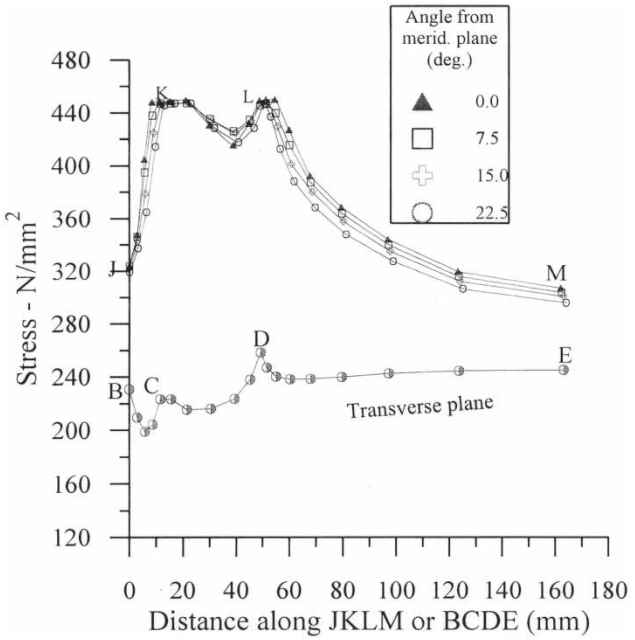

Fig. 9 Meridional effective stresses at ov = 30 per cent

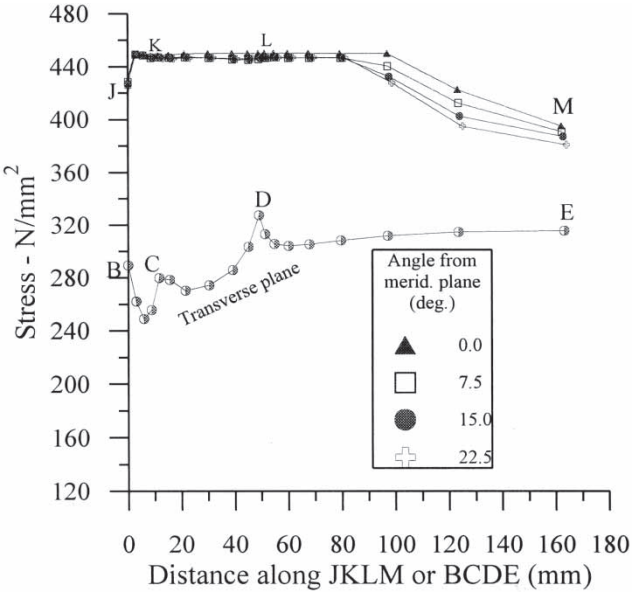

Fig. 10 Meridional effective stresses at ov = 65 per cent

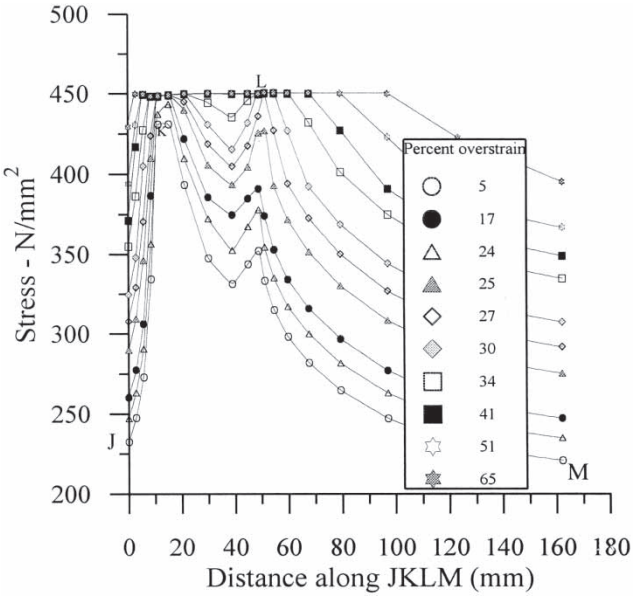

Fig. 12 Meridional effective stresses for varying ov

influence the local stress distributions even in the case of elastic–plastic loading. Figure 11 shows the meridional plane ov hoop stresses as ov is increased. The stress at point L increases very rapidly, whereas that at point K increases only marginally. This is because point K has already yielded while point L is still elastic. Further increase in ov causes the stress at point K to decrease progressively. Once point L has yielded, the stress starts to decrease with further ov. At ov = 65 per cent, the mid-section of curve KM has the highest stresses. Figure 12 shows the corresponding effective stress curves. At ov = 41 per cent, all the nodes on line KL have yielded.

The incipient yield pressure was determined by yielding the element around point t along line KL, for various k and d. The variations of incipient yield pressure with d are shown in Fig. 13. The lower k cylinders have lower incipient yield pressure. The results serve as a good guide when intending to carry out ov, and they indicate the pressure below which initial yielding of the structure may not be expected. They can also be used in service to guard against over pressure even when the structure is designed for elastic service. The ov = 5 per cent pressure curves are shown in Fig. 14 and have patterns similar to those in Fig. 13, although the

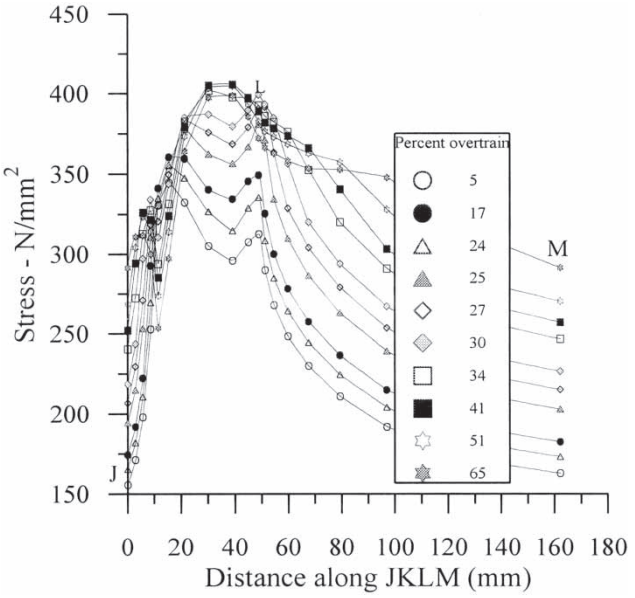

Fig. 11 Meridional hoop stresses for varying ov

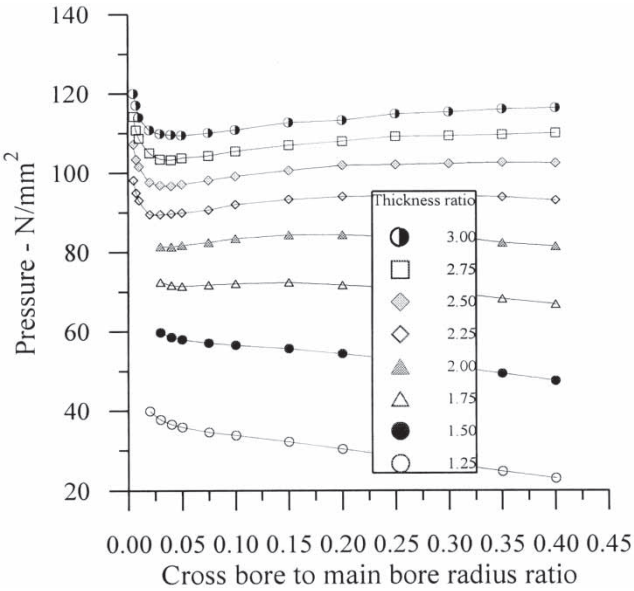

Fig. 13 Incipient yield pressure versus d

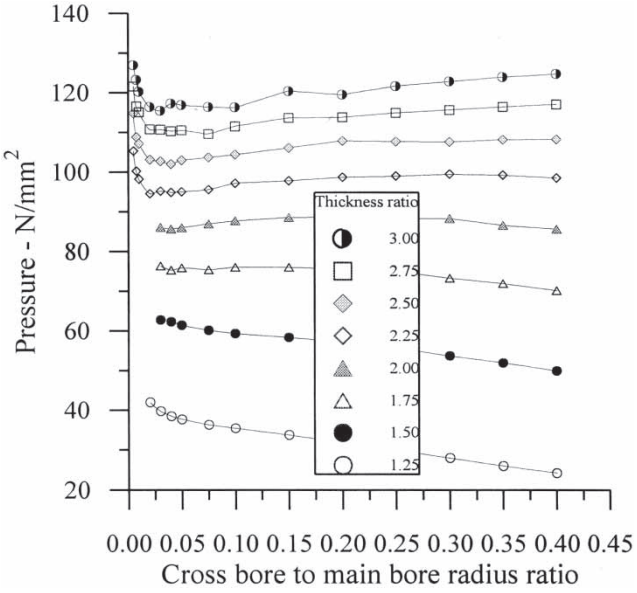

Fig. 14 Overstrain pressure versus d at ov = 5 per cent

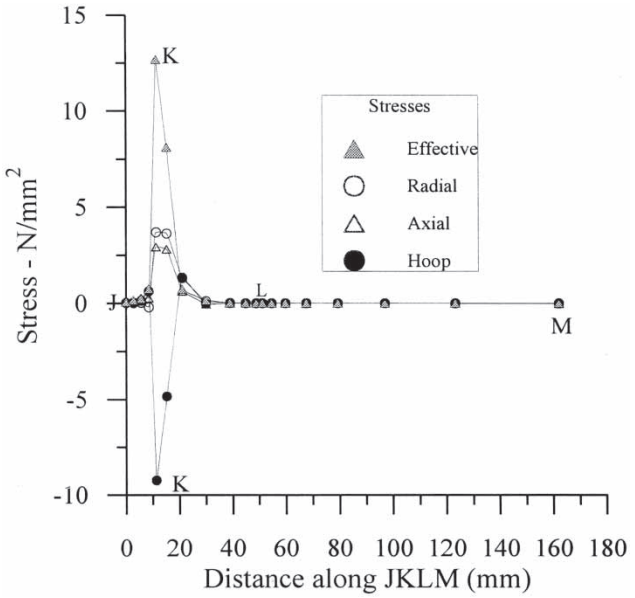

Fig. 16 Meridional residual stresses at ov = 5 per cent

pressure levels are higher. The incipient yield pressure curves are smooth, whereas these curves are not. This may be attributed to the 5 per cent yield condition used in this work. A more stringent yield condition would result in smooth curves. However, the time taken by using a stringent condition does not warrant the gain in accuracy [**37**]. Figure 15 shows the variation of ov pressure with ov. Although the ov pressure increases with the increase of ov, there is a drop in the pressure as ov increases from 17 to 24 per cent. This is because point L has a local maximum effective stress.

4.2 Residual stresses

Figure 16 shows the meridional plane residual stresses at ov = 5 per cent. Most of the stress values are zero except around point K. Although point K is not the point of maximum ov hoop stress, it is the point of maximum residual stress. The meridional residual hoop stresses for varying ov are shown in Fig. 17. The maximum value occurs at point K and this maximum increases with increasing ov. Figure 18 shows the corresponding effective stresses. Although a high value of residual hoop stress is desirable, the accompanying high value of residual effective stress is to be avoided

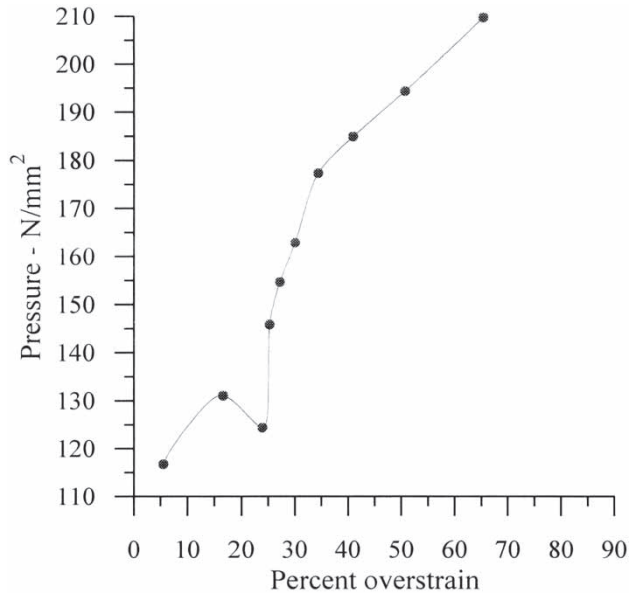

Fig. 15 Pressure versus ov

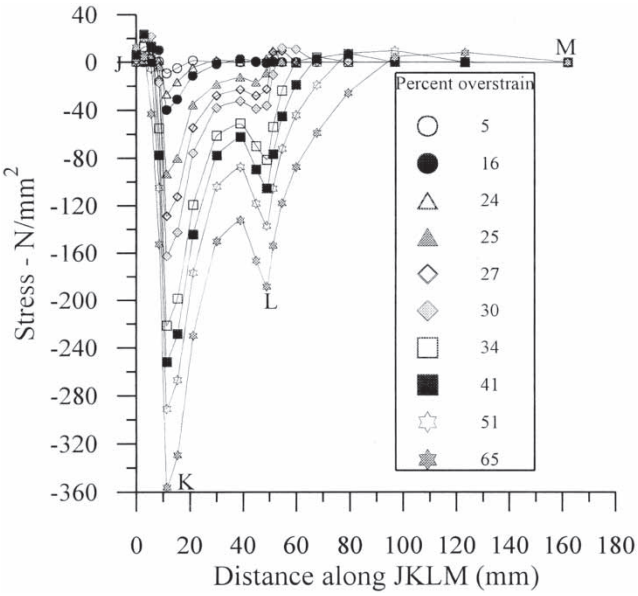

Fig. 17 Meridional residual hoop stresses for varying ov

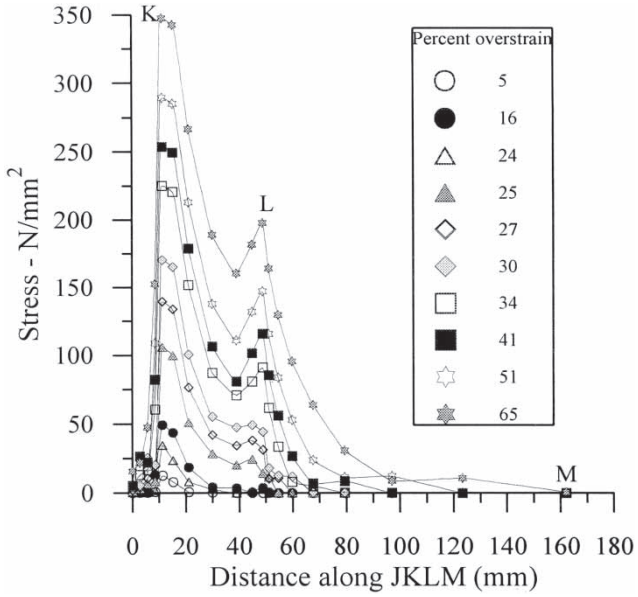

Fig. 18 Meridional residual effective stresses for varying ov

because reverse yielding is likely to take place. Figure 19 shows the variation of minimum residual hoop stress with d for $k = 1.25$–3. The curves for each k are not smooth. This phenomenon has been observed and discussed for plain and radiused entry cross-bored cylinders [**5**]. As a group of curves, a general relationship represented by a polynomial curve (of fifth order) is observed. Figure 20 represents the variations of minimum residual hoop stress with increase of ov and is similar to Fig. 15.

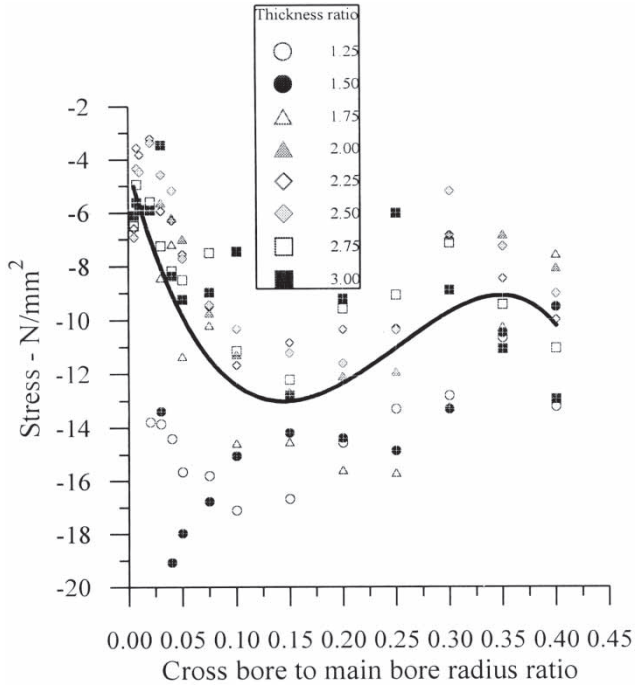

Fig. 19 Minimum residual hoop stresses versus d

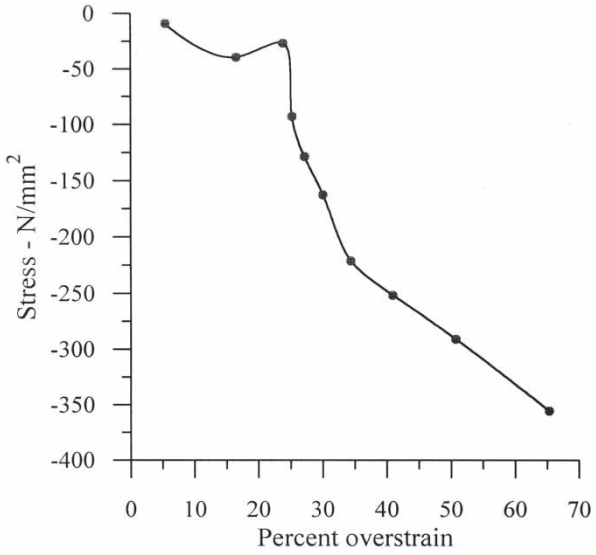

Fig. 20 Minimum residual hoop stresses versus ov

4.3 Service stresses

Figure 21 shows the in-service meridional hoop stresses after autofrettage and compared to the elastic stress levels for an internal pressure of 46.2 N/mm^2. A selected number of ov values are considered. The higher ov curves give more favourable hoop stress levels. For ov >5 per cent, point K has the lowest hoop stress, with this value decreasing with an increase in ov. The stress gradients on both sides of point K are very high and this is not desirable. Even though low values of hoop stress exist in service, the hoop stress distribution is not more favourable than in the case of elastic loading. For ov >5 per cent, point v becomes the point of maximum hoop stress. For ov >27 per cent, the hoop stress at point K may be expected to have a negative

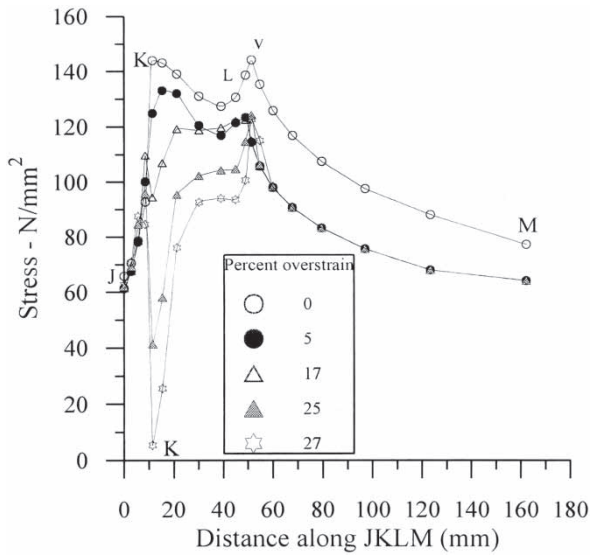

Fig. 21 Service hoop stresses for varying ov

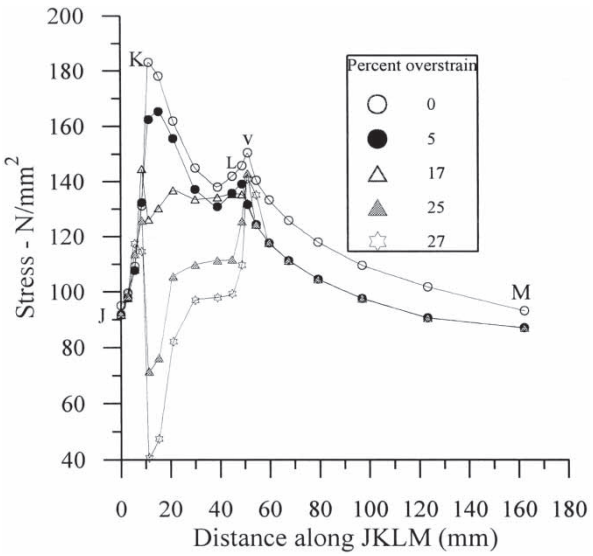

Fig. 22 Service effective stresses for varying ov

value. This could be a desirable outcome, particularly if any suspected cracks exist around this point, as the negative hoop stress tends to close the cracks and arrest any propagation. Stress reversals would also be avoided. Although high ov is desirable, care should be taken to ensure that it does not result in gross deformation. For high ov, the process of offloading must also proceed with strict safety procedures to avoid a collapse in the presence of the high pressures involved. Figure 22 shows the in-service meridional effective stress levels after autofrettage. The effective stresses around point K decrease with increasing ov. The effective stress gradients around point K are also very high. For ov >17 per cent, point v has the highest effective stress.

5 CONCLUSIONS AND RECOMMENDATIONS

At ov $= 5$ per cent, the ov effective stresses in the transverse plane were of the same magnitude, but much lower than those in the meridional plane. As ov increased, the main bore chamfer end had higher hoop stress than the cross-bore chamfer end in the meridional plane. At the cross-bore chamfer end, there was a local maximum hoop and effective stress. In the meridional and transverse planes, between the two chamfer ends, the maximum hoop stress occurred in nodes located about $\sim 7.5^\circ$ from each plane. This observation was found to require further investigation in future work. The meridional plane through thickness yielding at ov $= 41$ per cent should be avoided, to avert gross deformation and possible reverse yielding. With increased ov, the main bore chamfer end had the minimum residual hoop stress, and sharp stress gradients existed around this point. For ov > 30 per cent, high hoop stress gradients occurred at the cross-bore chamfer end. The minimum residual hoop stress increased with ov, the maximum being at the main bore chamfer end and a local maximum at the cross-bore chamfer end. Autofrettaging resulted in favourable residual stress levels, although stress distributions in service were not favourable due to the presence of sharp stress gradients at the main bore chamfer end. For ov >17 per cent, the highest service effective stress occurred at point v. For ov >27 per cent , hoop stress reversals are avoided and therefore ratcheting or incremental collapse is unlikely. Shakedown would be achieved at this ov. A compromise ov is required to avoid both high service stress gradients and stress reversals.

For the full benefits of ov to be realized, it is recommended that the cross-bore and chamfer be introduced after autofrettage of the plain cylinder and an FEM program developed for this analysis. The results of this research will be presented in a future article. It is also recommended that research be carried out to determine if nodes rather than elements should be the basis of yielding for more accurate solutions. The results of this research will also be presented in a future article.

REFERENCES

1 **Zapfec, C. A.** Boiler embrittlement. *Trans. ASME*, 1942, **66**(2), 81–126.
2 **Bush, S. H.** Statistics of pressure vessel and piping failures. *J. Press. Vessel Technol.*, 1988, **110**, 225–233.
3 **Iwadate T., Chiba K., Watanabe J., Mima S., Tokai K.,** and **Takedo H.** Safety analysis at a cross bore corner of high pressure polyethylene reactors. International Conference of Pressure Vessels and Piping: Materials, Nuclear Engineering and Solar Energy. *Trans. ASME*, 1981, **103**, 117–125.
4 **Masu, L. M.** *The effect of cross bore geometry on the strength of pressure vessels*. PhD Thesis, University of Leeds, 1989.
5 **Kihiu, J. M.** *Numerical stress characterization in cross-bored thick walled cylinders under internal pressure*. PhD Thesis, University of Nairobi, 2002.
6 **Ford, H., Watson, E. H.,** and **Crossland, B.** Thoughts on a code of practice for forged high pressure vessels of monobloc design. *Trans. ASME*, 1981, **103**, 2–8.
7 **Faupel, J. H.** and **Harris, B.** Stress concentrations in heavy walled cylindrical pressure vessels. *J. Ind. Eng. Chem.*, 1957, **49**, 1979–1986.
8 **Faupel, J. H.** Yield and bursting characteristics of heavy-wall cylinders. *Trans. ASME*, 1956, **78**(5), 1031–1064.
9 **Davies, L. M., Garne, L.,** and **Collier, J. G.** Second marshall study group on PWR pressure vessel integrity. *J. Press. Vessel Technol.*, 1983, **105**, 53–57.
10 **Kihiu, J. M., Mutuli, S. M.,** and **Rading, G. O.** Stress characterization in autofrettaged thick walled cylinders. *Int. J. Mech. Eng. Education*, University of Manchester, 2003, **31**(4), 370–389.

11 **Jorgensen, S. M.** Overstrain tests on thick walled cylinders. *J. Eng. Ind.*, 1960, **82**, 103–121.
12 **Faupel, J. H.** and **Furbeck, A. R.** Influence of residual stresses on behaviour of thick walled closed-end cylinders. In Proceedings of the 7th National Instruments Conference, Cleveland, Ohio, 9–10 September 1952.
13 **Lé, N. V.** Method and mechanism of beneficial residual stresses in tubes. *J. Press. Vessel Technol.*, 1994, **116**, 175–178.
14 **Marcal, P. V.** A stiffness method for elastic–plastic problems. *Int. J. Mech. Sci.*, 1965, **7**, 220–238.
15 **Yamada, Y., Yashimura, N.,** and **Sakurai, T.** Plastic stress–strain matrix and its application for the solution of elastic–plastic problems by the finite element method. *Int. J. Mech. Sci.*, 1968, **10**, 343–354.
16 **Owen, D. R. J.** and **Salonen, E. M.** Three dimensional elastic–plastic finite element analysis. *Int. J. Num. Meth. Eng.*, 1975, **9**, 209–218.
17 **Tomita, Y., Shindo, A.,** and **Nagai, M.** Axisymmetric deformation of circular elastic–plastic tubes under axial tension and internal pressure. *Int. J. Mech. Sci.*, 1984, **26**(6–8), 437–444.
18 **Pillinger, I., Hartley, P., Sturgess, C. E. N.,** and **Rowe, G. W.** Use of mean normal technique for efficient and numerically stable large strain elastic–plastic finite element solutions. *Int. J. Mech. Sci.*, 1986, **28**(1), 23–29.
19 **Steele, M. C.** Partially plastic thick-walled cylinder theory. *J. Appl. Mech.*, 1952, **19**, 133–140.
20 **Masu, L. M.** Plasticity analysis and cross bore size effects on the fatigue strength of thick walled cylinders. *E. Afr. J. Eng.*, 1994, **1**(2), 22–23.
21 **Tan, C. L.** Stress distributions in thick walled cylinders due to the introduction of bore after autofrettage. *J. Strain Analysis*, 1986, **21**, 177–183.
22 **Jorgensen, S. M.** Overstrain and bursting strength of thick-walled cylinders. *Trans. ASME*, 1958, **80**(3), 561–570.
23 **Dudans, Z.** Finite element incremental elastic-plastic analysis in pressure vessels. *J. Eng. Ind.*, 1970, **92**, 293–302.
24 **Hsu, L. C.** *Analysis for design. Part 1. Introduction: pressure vessels and piping: design and analysis*. Vol. 1. Analysis, 1972 (ASME, United Engineering Centre, New York).
25 **Hussain, M. A., Pu, S. L., Vasilakis, J. D.,** and **O'Hara, P.** Simulation of partial autofrettage by thermal loads. *J. Press. Vessel Technol.*, 1980, **102**, 314–318.
26 **Zhou, H.** and **Rao, M. D.** On the error analysis of residual stress measurements by the hole drilling method. *J. Strain Analysis*, 1993, **28**(4), 273–276.
27 **Sharman, D. J., Stark, H. L.,** and **Kelly, D. W.** Bench marking of a destructive technique to determine residual stresses in thick walled axisymmetric components. *J. Strain Analysis*, 1997, **32**(2), 87–96.
28 **Sharman, D. J., Stark, H. L.,** and **Kelly, D. W.** A comparison of potential methods for the alleviation of residual stresses in the necks of aluminium alloy thick-walled gas cylinders. *J. Strain Analysis*, 1997, **32**(5), 315–323.
29 **Perl, M.** and **Aroné, R.** An axisymmetric stress release method for measuring the autofrettage level in thick-walled cylinders – part I: basic concept and numerical simulation. *J. Press. Vessel Technol.*, 1994, **116**, 384–388.
30 **Chen, P. C. T.** The Bauschinger and hardening effects on residual stresses in an autofrettaged thick walled cylinder. *J. Press. Vessel Technol.*, 1986, **108**, 109–112.
31 **Rees, D. W. A.** Autofrettage theory and fatigue life of open ended cylinders. *J. Strain Analysis*, 1990, **25**(2), 109–121.
32 **Jahed, H.** and **Dubey, R. N.** An axisymmetric method of elastic-plastic analysis capable of predicting residual stress field. *J. Press. Vessel Technol.*, 1997, **119**, 264–273.
33 **Kihiu, J. M.** and **Mutuli, S. M.** Time and space management in structural analysis problems. *Int. J. Mech. Eng. Edu.*, 1998, **26**(4), 273–292.
34 **Kihiu, J. M., Rading, G. O.,** and **Mutuli, S. M.** Geometric constants in plain cross-bored cylinders. *J. Press. Vessel Technol.*, 2003, **125**, 446–453.
35 **Kihiu, J. M., Rading, G. O.,** and **Mutuli, S. M.** Overstraining in flush plain cross-bored cylinders. *Proc. Instn Mech. Engrs, Part C: J. Mechanical Engineering Science*, 2004, **218**(C2), 143–153.
36 **Kihiu, J. M., Rading, G. O.,** and **Mutuli, S. M.** Transition, convergence and constancy in radiused entry cross-bored cylinders. *Trans. Can. Soc. Mechanical Engineers*, 2004, **28**(2B), 343–353.
37 **Kihiu, J. M., Rading, G. O.,** and **Mutuli, S. M.** Overstrain in flush radiused entry cross-bored cylinders. *J. Strain Analysis*, 2005, submitted for publication.
38 **Kihiu, J. M., Rading, G. O.,** and **Mutuli, S. M.** Universal SCFs in optimal chamfered cross-bored cylinders. *Int. J. Press. Vessels Piping*, 2005, submitted for publication.
39 **Mraz, G. J.** and **Nisbett, E. G.** Design, manufacture and safety aspects of forged vessels for high pressure service. *J. Press. Vessel Technol.*, 1980, **102**, 99–106.
40 **Irons, B. M.** A frontal solution program. *Int. J. Num. Meth. Eng.*, 1970, **2**, 5–32.
41 **Hinton, E.** and **Campbell, J. S.** Local and global smoothing of discontinuous finite element function using a least square method. *Int. J. Num. Meth. Eng.*, 1974, **8**, 461–480.

APPENDIX

Notation

ASME	American Society of Mechanical Engineers
C	material constant
ca	chamfer angle
clr	chamfer length ratio
d	cross-bore to main bore radius ratio
FEM	finite-element method
k	thickness ratio
n	strain hardening exponent
ov	overstrain
u_x	displacement in x-direction
u_y	displacement in y-direction
u_z	displacement in z-direction
Y_S	yield stress
$\overline{\varepsilon^n}$	effective strain
$\overline{\sigma}$	effective stress